

## COTR RESISTANT PROFILE MONITOR\*

H. Loos<sup>†</sup>, SLAC National Accelerator Laboratory, Menlo Park, CA 94025, U.S.A.

### Abstract

Electron beam accelerators used as drivers for short wavelength FELs need ultra-high brightness beams with small emittances and highly compressed bunch lengths. The acceleration and beam transport process of such beams leads to micro-bunching instabilities which cause the emergence of coherent optical transition radiation (COTR). The effect of COTR on profile monitors based on OTR or fluorescent screens can be quite detrimental to their intended use to measure beam sizes and profiles. This presentation will review past observations of the beam diagnostics issues due to COTR and discuss various mitigation schemes for profile monitors as well as present experience with such implementations.

### INTRODUCTION

Free electron laser facilities for the generation of soft and hard x-rays [1–5] utilize high brightness linear accelerators which have to produce electron beams of exceptional quality to achieve lasing in a feasible length of undulator. The beams of multi-GeV energy need to have sub-micrometer transverse emittance,  $10^{-4}$  energy spread and 10s of fs or even shorter bunch durations for a total charge of the order of few 100 pC. Such parameters necessitate the measurement of transverse beam sizes and profiles from the injector area all the way to the undulators to establish beam emittance measurements throughout the accelerator so that machine tuning and optimization to maintain the high brightness beam into the undulators becomes possible. Furthermore, the 2-dimensional transverse beam distribution is needed to diagnose transverse coupling and to measure the time-resolved beam size or energy spread in conjunction with a transverse deflecting structure [6]. The most convenient method to obtain images of the transverse beam distribution is to use a profile monitor, i.e. a screen of some material intercepting the electron beam and emitting visible light imaged onto a CCD camera. The small, typically only several 10s of  $\mu\text{m}$  beam sizes make the use of scintillating crystals or thin foils generating optical transition radiation (OTR) [7] advantageous. The latter method was envisioned as the main transverse beam diagnostic for many XFEL accelerators because of the instantaneous response of OTR, and the absence of charge density dependent saturation effects or image resolution diluting depth effects as for thick scintillating crystals [8].

The ultra-high brightness of the XFEL accelerators—needed to enable coherent radiation at x-ray wavelengths—however poses a challenging problem for transverse beam diagnostics as became apparent for the first time during the

commissioning of the LCLS injector [9]. It became obvious then that imaging beam distributions using OTR screens can lead to completely unreliable results due to coherent effects from the longitudinal structure in the bunch distribution, i.e. the emission of coherent optical transition radiation (COTR).

The following sections first provide a brief summary of the COTR issue, then a review of various mitigation schemes to provide images of the beam distribution that are not affected by COTR artifacts, and concluding with results from tests of the PSI design profile monitor at SwissFEL and LCLS.

### COTR OBSERVATIONS

Coherent optical transition radiation is the process by which the light emission of a charged particle intercepting the boundary between two different media is not just the sum of the intensity of the light from individual particles as desired for OTR based beam diagnostics, but where longitudinal structure in the bunch at visible wavelengths leads to a coherent superposition of the emitted light fields, and hence an increase of the light intensity which can be a factor up to the number of particles if the bunch length itself is shorter than visible wavelengths.

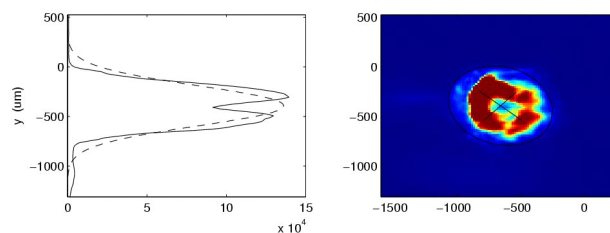


Figure 1: An image of the COTR radiation in the LCLS injector after BC1 observed with extreme bunch compression. From [9].

The initial observation of COTR [10] occurred in a deliberate way from an electron beam temporally modulated by the SASE process at visible wavelengths, which lead to the coherent enhancement of the incoherent OTR intensity by several orders of magnitude within the narrow SASE bandwidth. The first observation of broadband visible COTR at LCLS [9, 11] as shown in Fig. 1 was unexpected, but soon explained as a result of micro-bunching induced by the longitudinal space charge instability [12]. Subsequently the COTR effect has also been documented at most other high-brightness accelerators, both equipped with photo or thermionic cathode guns [13–16], with the latter requiring several bunch compression stages. Summaries of these observations can be found in [14, 17].

There are several implications of the COTR effect on the beam profile measurement. The light intensity can be greatly increased from a small factor for uncompressed

\* Work supported by US DOE contract DE-AC02-76SF00515.

<sup>†</sup> loos@slac.stanford.edu

beams of ps duration to up to 5 orders of magnitude for highly compressed bunches with current spikes of few fs duration, even leading to CCD damage. Figure 2 shows the intensity enhancement for different bunch compression settings at FLASH [14]. For longer bunches, spurious changes to the measured OTR beam size can be observed which are not related to the actual beam size, but rather stem from non-uniform coherent enhancement across the transverse beam profile. Lastly, the entire transverse shape of the light distribution can change so that the COTR distribution from a Gaussian electron beam profile becomes a doughnut-shaped ring structure for bunches exhibiting sufficient transverse correlation of the longitudinal micro-bunching or current spikes (see Fig. 1).

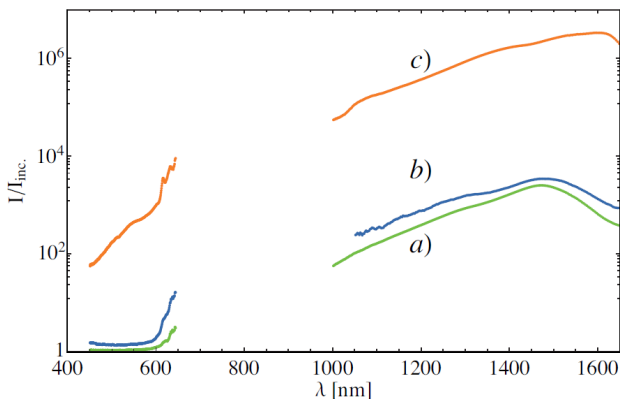


Figure 2: Visible and near IR relative spectral intensities of COTR w.r.t. incoherent OTR for three different bunch compression setups at FLASH. From [14].

### COTR MITIGATION

A great number of methods has been proposed or tested over the last years to circumvent the detrimental coherent effects occurring when a high-brightness electron beam intercepts a screen, and to provide an image of the electron beam that is strictly proportional to its transverse charge density distribution. The schemes address this by changing one or more parameters in the OTR imaging process. The electron beam itself can be tailored to suppress its coherence, or the OTR emission can get spatially or spectrally filtered, or a different physical process to generate a beam distribution image can be chosen to avoid the sensitivity to the longitudinal particle distribution. The challenge for all the schemes is to overcome the potentially many orders of magnitude dominance of the COTR over the desired radiation process, considering that just an equal or even lesser fraction of COTR can already significantly alter measured beam profiles.

#### Beam Manipulation

As the LSC instability is driven by a small slice energy spread, one expects the inclusion of a laser heater in the injector of an accelerator to mitigate or sufficiently suppress

the COTR emission by increasing the energy spread of the beam. Such suppression has indeed been observed [18] with the COTR intensity after the second LCLS bunch compressor being lowered by two orders of magnitude, however still a factor 6 above the incoherent level (see Fig. 3) with OTR beam sizes not representative of the true electron beam distribution.

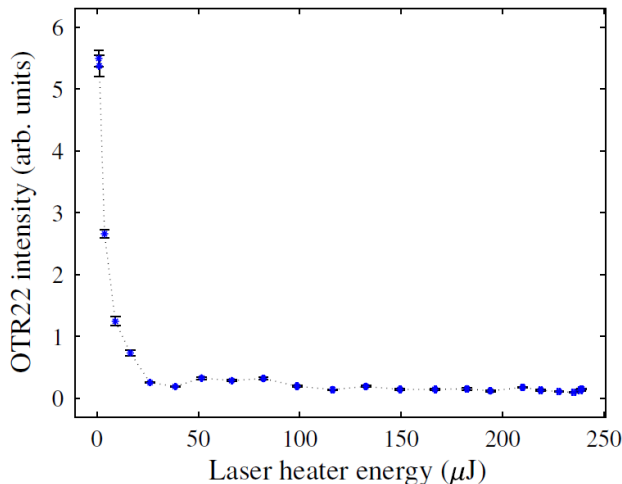


Figure 3: Reduction of COTR intensity at LCLS after the second bunch compressor with increasing laser heater power. From [18].

In the LCLS injector the required chicane for the laser heater manifests itself already the LSC instability due to the 8 mm  $R_{56}$ . As shown in Fig. 4 the OTR light intensity downstream of the laser heater doubles with just the chicane turned on, but is still about 25% above the incoherent OTR when the beam is heated by the laser [19]. Also an artificially 30% lower projected beam emittance is measured with just the chicane turned on [20], the effect on the measured emittance of smaller COTR effect with the heater on has not yet been determined.

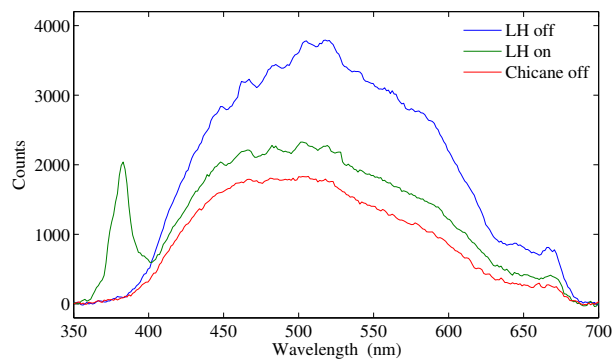


Figure 4: OTR spectrum after LCLS injector laser heater of 135 MeV beam and 150 pC charge. Incoherent spectrum with heater chicane turned off.

A different approach to change the beam phase space to suppress COTR emission was proposed in [21] for typical

injector beam energies. In this scheme a thick foil acts both as a spoiler to substantially increase the beam divergence and as the beam exits the foil to generate backwards OTR which is viewed via a downstream mirror. The increased beam divergence broadens the far-field COTR distribution which is equivalent to state that it limits the COTR source size and hence the ability of different parts of the beam to radiate coherently. While no direct implementation of this scheme has been reported, the suppression of COTR on downstream OTR screens by spoiling the beam emittance with inserted upstream OTR foils was observed at LCLS. The scheme has however limitations for high GeV beams where the required spoiler thickness to sufficiently increase the beam divergence becomes impractical.

### Selective OTR Filtering

The different characteristics of OTR and COTR in terms of angular and spectral distribution can be utilized to preferably detect the OTR component and to suppress the COTR part. These techniques are also important for the use of scintillators as such crystals also represent a media boundary which emits OTR and consequently COTR.

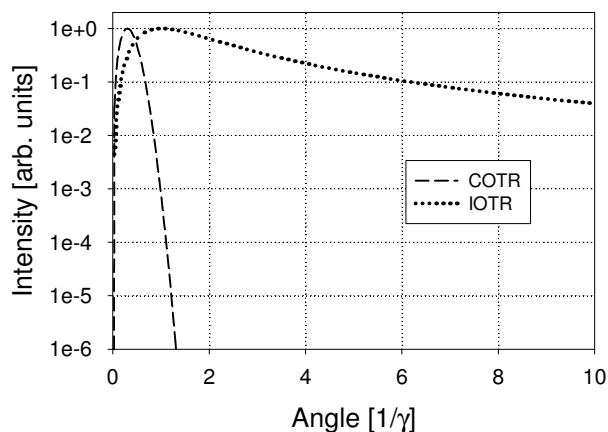


Figure 5: Comparison of the far-field angular emission distribution of COTR and incoherent OTR for an electron beam with 250 MeV LCLS beam parameters. From [22].

COTR is emitted from a larger source dimension than the OTR point spread function, and this size can be as large as the beam size for fully transverse coherent micro-bunching. This leads to a much narrower angular distribution of the COTR which can be exploited by spatially blocking the narrow COTR far-field cone in the Fourier plane of an imaging setup, while allowing the larger spatial frequencies of the incoherent OTR to pass.

The principle as proposed in [22] is shown in Fig. 5 where in case of the LCLS injector at 250 MeV the COTR emitted by the entire transverse extent of the beam is already completely suppressed within the  $1/\gamma$  cone of the incoherent OTR. COTR emitted from smaller fractions of the transverse beam profile would however have much larger divergence and therefore be suppressed to a much lesser extent. Although no direct experimental verification of this scheme for

ISBN 978-3-95450-134-2

OTR screens has been reported, it is now used in many scintillator screen applications to suppress COTR as described in the following section.

The strong wavelength dependence of the COTR as shown in Fig. 2 which has increasing intensity towards longer wavelength from the LSC instability gain [12] suggests spectral filtering of the OTR at shorter wavelengths where the relative COTR contribution can be smaller [13]. The COTR observed at the APS injector from a compressed beam at 325 MeV could be suppressed using a narrow bandpass filter at 400 nm, and the fluorescence from an LSO:Ce scintillator crystal did not exhibit any coherent effects.

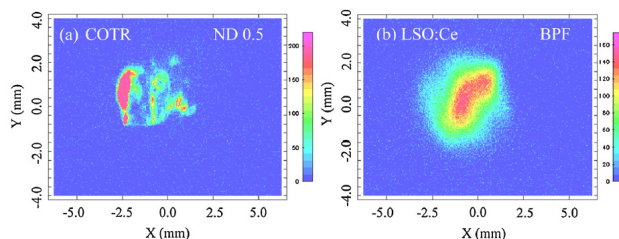


Figure 6: Spectral COTR mitigation using a 400 nm bandpass filter at the APS injector. From [13].

While this scheme can be successful for certain beam conditions with no micro-bunching gain at the blue end of the spectrum, it cannot be applied generally for highly compressed bunches with strong COTR intensity in the entire visible spectrum and possible beyond into the UV from few fs long current spikes. Much shorter wavelengths for OTR are necessary to utilize a spectral range with negligible bunching form-factor contributions.

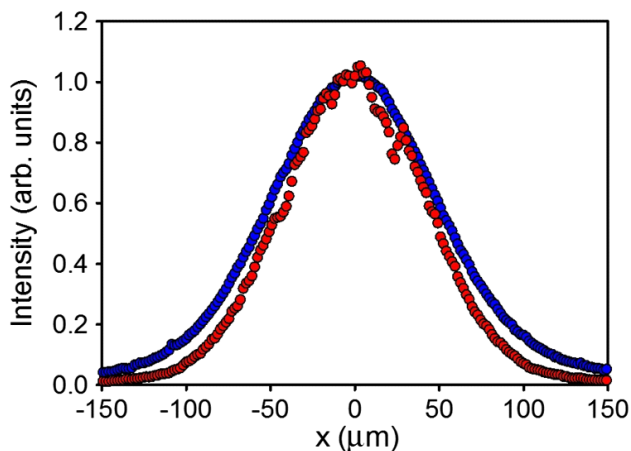


Figure 7: OTR beam profiles measured in the visible (blue) and in the EUV (red) for 855 MeV beam at MAMI. From [23].

Such OTR imaging has been proposed and demonstrated in the EUV [23]. As the OTR yield from a foil is essentially determined by the reflectivity at the respective wavelength, this is not a critical issue in the visible when using a metal foil, but becomes important at much shorter wavelengths. In this experiment at MAMI, a molybdenum target was used at a

grazing incidence angle for high reflectivity, and a multilayer spherical mirror was used to image the OTR onto a CCD camera. The reported somewhat smaller beam sizes in the EUV compared to the visible range are shown in Fig. 7 and not yet fully understood. Although demonstrated as a viable beam size diagnostics, the complexity of the necessary in-vacuum setup makes this diagnostics not attractive for widespread use in an accelerator with multiple beam imaging stations.

### OTR Avoidance Schemes

The most successful COTR mitigation scheme has been to avoid using OTR all together and instead use physical processes which do not probe the electron beam's Coulomb field at visible wavelengths. This is usually done via the detection of bremsstrahlung induced beam energy loss via scintillators or beam loss signal detection in wire scanners. The latter has been the main diagnostics where the observation of COTR made already installed OTR screens unreliable, e.g. at LCLS, but they only provide beam profiles and not images. Another mechanism which has been proposed is to use parametric x-rays (PXR) to generate a photon distribution proportional to the beam charge distribution which is then detected with a scintillator [24]. Since hard x-rays would be generated, the diagnostics should be impervious to coherence effects.

The renaissance of the scintillator raises again issues of resolution for small beam sizes and saturation for high charge densities as they were originally investigated [8]. Both were conveniently absent from OTR diagnostics which is only limited in resolution by the point spread function of typically sub-10  $\mu\text{m}$ , and in charge density by material damage.

The scintillator resolution is mainly limited due to the crystal thickness and viewing geometry because the entire path of the beam through the crystal acts as a line source. The choice of thinner crystals with free-standing ones available as thin as 20  $\mu\text{m}$  can shorten the length of the line source considerably and also limit beam losses from the beam interception with the crystal. The conventional geometry of a crystal oriented perpendicular to the beam with a downstream mirror or foil to direct the fluorescence away from the beam to a camera needs to be avoided to prevent additional COTR generation from the mirror. Extensive studies of the optimum viewing geometry without a mirror intercepting the beam as well were done in [25, 26] showing beam sizes measured from even a 300  $\mu\text{m}$  thick LYSO crystal close to the OTR measurement for a 15  $\mu\text{m}$  beam size as shown in Fig. 8. Even smaller vertical beam sizes of 7  $\mu\text{m}$  from a 50  $\mu\text{m}$  thick YAG crystal have been recently reported using a gated CCD [27].

Even when using a scintillating crystal, OTR and hence COTR are still generated at the entrance and exit boundaries of the crystal. The much larger efficiency of scintillators compared to OTR already provides a few orders of magnitude suppression. Furthermore, the same filtering as for OTR can be used here to suppress COTR much more effectively. Spatial filtering benefits from the nearly isotropic

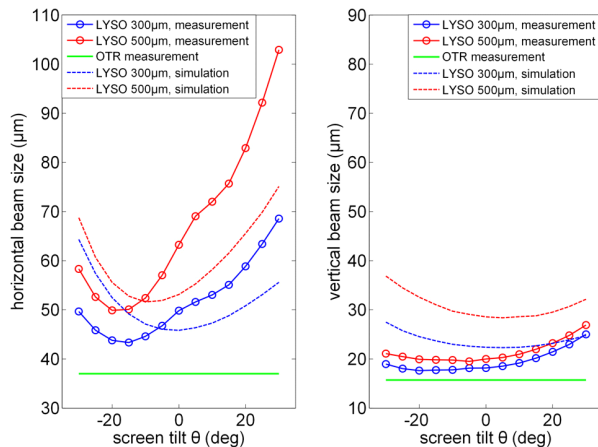
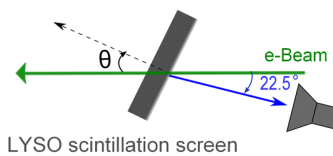


Figure 8: Measured beam sizes for LYSO crystals for various screen tilt angles compared to simulation and OTR measurement at MAMI. From [25].

light emission from the scintillator and the COTR can be suppressed with a mask blocking the central COTR cone [28] or by tilting the YAG crystal to direct both the COTR from the crystal surface and a preceding viewing mirror away from the lens of the camera [6, 29]. In both cases no COTR could be observed from the respective screens. The same spatial separation is also implemented in the later discussed PSI profile monitor [30].

Another effective method is to exploit the different time scales of the OTR and scintillation process. Whereas the OTR emission is prompt and happens within the duration of the bunch, the fluorescence in crystals typically used occurs with a lifetime of the order of 100 ns. By using a fast gated CCD camera, the trigger can be delayed w.r.t. the beam by 10s of ns so that the instantaneous COTR is blocked and only the fluorescent light emission is captured by the camera [31]. The complete disappearance of COTR effects from the LuAG screen can be seen in Fig. 9 when the camera trigger is delayed by 100 ns to the beam time.

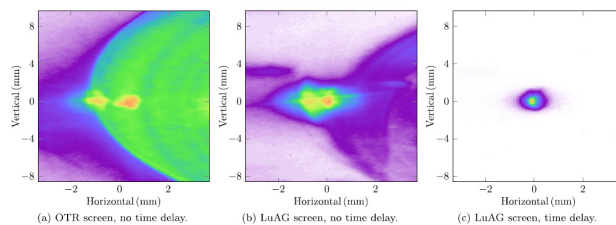


Figure 9: Beam images from OTR and LuAG screens for different trigger delays of a gated CCD showing COTR suppression in the delayed case at FLASH. From [31].



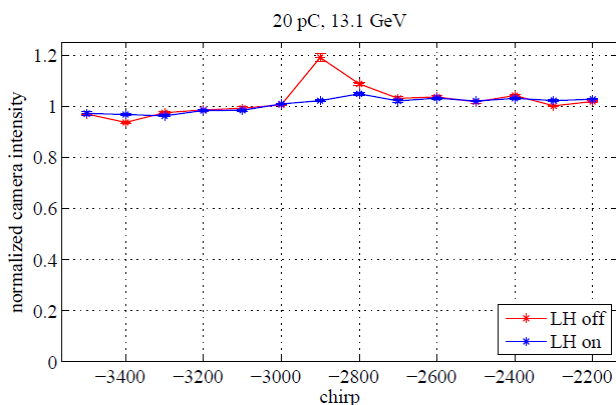


Figure 13: Integrated intensity from the PSI profile monitor at LCLS for different RF settings (chirp in MeV) at 20 pC charge. From [30].

Changing the accelerating RF phases and bunch compression, the suppression of COTR can be studied which is most prevalent at peak compression. Although no recent quantitative measurements of COTR at this location were available, it's presence could still be confirmed by the damage occurring to a CCD exposed to COTR from an OTR screen also mounted on the actuator as part of the PSI profile monitor. The results are shown in Figs. 13 and 14 at 13 GeV beam energy for 20 and 150 pC, respectively.

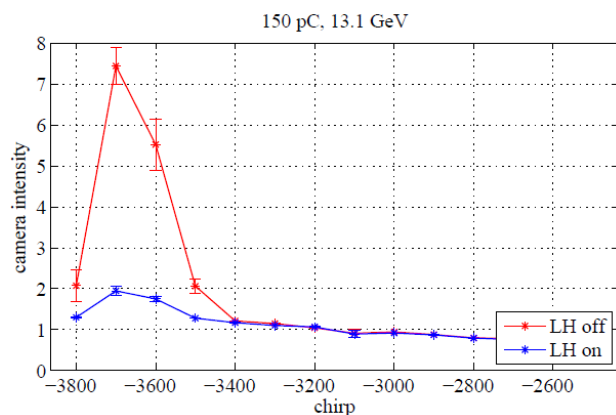


Figure 14: Same as previous figure for 150 pC. From [30].

Both measurements with the injector laser heater on and off are shown. For the low charge case, only a small increase in light intensity at the peak compression setting can be observed without the laser heater, which disappears completely when it is turned on. For the higher charge case, significant intensity enhancement by a factor of seven is still observed for the highest compression settings (corresponding to above 5 kA peak current) while for the normally used LCLS bunch compression settings of less than 4 kA only a minor change can be seen. When the laser heater is turned on, the enhancement at peak compression is reduced to less than a factor two, which can still be detrimental to beam size measurements. However, while previously the laser heater was only able to

partially suppress COTR on the LCLS OTR screens, now a complete suppression for most beam setups on the YAG screen can be achieved.

Presently, an upgrade is underway using a different in-vacuum mirror to avoid coherent diffraction radiation being emitted from the edge of the mirror which points directly towards the camera.

The remaining enhancement can be understood as fluorescence being incited in the crystal via bunch form-factor components in the UV or shorter wavelengths which generate coherent radiation traveling through the crystal at these wavelengths. Strong indication for this effect could also be observed in the beam overlap diagnostics used in the LCLS soft x-ray self-seeding setup [32] where the electron beam passes by a 20  $\mu\text{m}$  thick YAG crystal within a few mm. In the setup, an annular mirror prevents a direct path of coherent diffraction radiation from the crystal towards the camera, yet strong coherent light effects can be seen [19] which are also attributed to the same effect.

### SUMMARY

The coherence effects seen in high brightness accelerators for x-ray FELs have made the use of standard OTR screen unfeasible for most situations after the bunches have been compressed or LSC instability gain has created micro-bunching. Mitigation schemes for OTR screens themselves were not successful in fully suppressing COTR with the option remaining to move to much shorted detection wavelengths. However, scintillator screens have reemerged as a viable alternative with demonstrated resolution at the 10  $\mu\text{m}$  level. Temporal and spatial separation have been demonstrated to sufficiently suppress COTR in most cases. Scintillator screens using spatial COTR separation schemes are now planned for several XFEL projects under construction.

### REFERENCES

- [1] P. Emma, R. Akre, J. Arthur, R. Bionta, C. Bostedt, *et al.* Nature Photon. 4 (2010), 641.
- [2] T. Ishikawa, *et al.* Nature Photon. 6 (2012), 540.
- [3] *The european x-ray free-electron laser technical design report.* Technical Report DESY 2006-097, DESY (2007).
- [4] H. S. Kang, K.-W. Kim, I. S. Ko. Proceedings of the 2015 International Particle Accelerator Conference, Richmond, VA. p. WEYC2 (2015).
- [5] *SwissFEL conceptual design report.* Technical Report 10-04, Paul Scherrer Institut (2012).
- [6] C. Behrens, F.-J. Decker, Y. Ding, V. Dolgashev, J. Frisch, *et al.* Nature Commun. 5 (2014), 3762.
- [7] B. Yang, J. L. Bailey, D. R. Walters, S. J. Stein. Proceedings of the 2005 Particle Accelerator Conference, Knoxville, TN. pp. 4209–4211 (2005).
- [8] A. Murokh, J. Rosenzweig, I. Ben-Zvi, X. Wang, V. Yakimenko. Proceedings of the 2001 Particle Accelerator Conference, Chicago, IL. pp. 1333–1335 (2001).
- [9] R. Akre, D. Dowell, P. Emma, J. Frisch, S. Gilevich, *et al.* Phys. Rev. ST Accel. Beams 11 (2008), 030703.

- [10] A. H. Lumpkin, R. Dejus, J. Lewellen, W. Berg, S. Biedron, *et al.* Phys. Rev. Lett. 88 (2002), 234801.
- [11] H. Loos, *et al.* Proceedings of the 2008 FEL Conference, Gyeongju, Korea. pp. 166–172 (2008).
- [12] D. Ratner, A. Chao, Z. Huang. Proceedings of the 2008 FEL Conference, Gyeongju, Korea. pp. 338–341 (2008).
- [13] A. Lumpkin, N. Sereno, W. J. Berg, M. Borland, Y. Li, *et al.* Phys. Rev. ST Accel. Beams 12 (2009), 080702.
- [14] S. Wesch, B. Schmidt. Proceedings of the 2011 DIPAC Conference, Hamburg, Germany. pp. 539–543 (2011).
- [15] S. Weathersby, M. Dunning, C. Hast, K. Jobe, D. McCormick, *et al.* Proceedings of the 2011 PAC Conference, New York, NY. pp. 2426–2428 (2011).
- [16] K. Togawa, *et al.* Proc. of the Fifth Microbunching Instability Workshop, Pohang, Korea (2013).
- [17] A. H. Lumpkin. Proceedings of the 2013 FEL Conference, New York, NY. pp. 169–172 (2013).
- [18] Z. Huang, A. Brachmann, F.-J. Decker, Y. Ding, D. Dowell, *et al.* Phys. Rev. ST Accel. Beams 13 (2010), 020703.
- [19] H. Loos. Proceedings of the 2014 IBIC Conference, Monterey, CA. pp. 475–485 (2014).
- [20] F. Zhou, K. Bane, Y. Ding, Z. Huang, H. Loos, *et al.* Phys. Rev. ST Accel. Beams 18 (2015), 050702.
- [21] A. Murokh, E. Hemsing, J. Rosenzweig. Proceedings of the 2009 Particle Accelerator Conference, Vancouver, BC. pp. 3991–3993 (2009).
- [22] R. B. Fiorito. Proceedings of the 2009 Particle Accelerator Conference, Vancouver, BC. pp. 741–745 (2009).
- [23] L. G. Sukhikh, G. Kube, S. Bajt, W. Lauth, Yu, *et al.* Phys. Rev. ST Accel. Beams 17 (2014), 112805.
- [24] A. Gogolev, A. Potylitsyn, G. Kube. Journal of Physics: Conference Series 357 (2012), 012018.
- [25] M. Yan, C. Behrens, C. Gerth, G. Kube, B. Schmidt, *et al.* Proceedings of the 2011 DIPAC Conference, Hamburg, Germany. pp. 440–442 (2011).
- [26] G. Kube, C. Behrens, C. Gerth, B. Schmidt, M. Yan, *et al.* Proceedings of the 2012 IPAC Conference, New Orleans, LA. pp. 2119–2121 (2012).
- [27] T. Naito, T. Mitsuhashi. Proceedings of the 2014 IBIC Conference, Monterey, CA. pp. 426–429 (2014).
- [28] H. Tanaka. Proceedings of the 2011 IPAC Conference, San Sebastian, Spain. pp. 21–25 (2011).
- [29] H. Loos, *et al.* Proceedings of the 2010 Beam Instrumentation Workshop, Santa Fe, NM. pp. 34–43 (2010).
- [30] R. Ischebeck, E. Prat, V. Schlott, V. Thominet, M. Yan, *et al.* Proceedings of the 2014 IBIC Conference, Monterey, CA. pp. 259–262 (2014).
- [31] C. Behrens, C. Gerth, G. Kube, B. Schmidt, S. Wesch, *et al.* Phys. Rev. ST Accel. Beams 15 (2012), 062801.
- [32] D. Ratner, R. Abela, J. Amann, C. Behrens, D. Bohler, *et al.* Phys. Rev. Lett. 5 (2015), 054801.